

RESEARCH PAPER



Hepatocyte CD36 modulates UBQLN1-mediated proteasomal degradation of autophagic SNARE proteins contributing to septic liver injury

Yanping Li^a, Jingyuan Xu^{a*}, Weiting Chen^{a*}, Xingxing Wang^{a*}, Zhibo Zhao^a, Yuqi Li^a, Linkun Zhang^a, Junkui Jiao^a, Qin Yang^a, Qiuying Ding^a, Ping Yang^a, Li Wei^a, Yao Chen^{a#}, Yaxi Chen^{a#}, Xiong Z. Ruan^{a,b#}, and Lei Zhao^{id a#}

^aCentre for Lipid Research & Chongqing Key Laboratory of Metabolism on Lipid and Glucose, Key Laboratory of Molecular Biology for Infectious Diseases (Ministry of Education), Institute for Viral Hepatitis, Department of Infectious Diseases, the Second Affiliated Hospital, Chongqing Medical University, Chongqing, China; ^bJohn Moorhead Research Laboratory, Centre for Nephrology, University College London Medical School, London, England, UK

ABSTRACT

Macroautophagy/autophagy plays a protective role in sepsis-induced liver injury. As a member of class B scavenger receptors, CD36 plays important roles in various disorders, such as atherosclerosis and fatty liver disease. Here we found that the expression of CD36 in hepatocytes was increased in patients and a mouse model with sepsis, accompanied by impaired autophagy flux. Furthermore, hepatocyte *cd36* knockout (*cd36*-HKO) markedly improved liver injury and the impairment of autophagosome-lysosome fusion in lipopolysaccharide (LPS)-induced septic mice. *Ubqln1* (ubiquilin 1) overexpression (OE) in hepatocyte blocked the protective effect of *cd36*-HKO on LPS-induced liver injury in mice. Mechanistically, with LPS stimulation, CD36 on the plasma membrane was depalmitoylated and distributed to the lysosome, where CD36 acted as a bridge molecule linking UBQLN1 to soluble N-ethylmaleimide-sensitive factor attachment protein receptor (SNARE) proteins and hence promoting the proteasomal degradation of SNARE proteins, resulting in fusion impairment. Overall, our data reveal that CD36 is essential for modulating the proteasomal degradation of autophagic SNARE proteins in a UBQLN1-dependent manner. Targeting CD36 in hepatocytes is effective for improving autophagic flux in sepsis and therefore represents a promising therapeutic strategy for clinical treatment of septic liver injury.

Abbreviations: AAV8: adeno-associated virus 8; AOSC: acute obstructive suppurative cholangitis; ATP1A1: ATPase, Na⁺/K⁺ transporting, alpha 1 polypeptide; CASP3: caspase 3; CASP8: caspase 8; CCL2: chemokine (C-C motif) ligand 2; *cd36*-HKO: hepatocyte-specific *cd36* knockout; Co-IP: co-immunoprecipitation; CQ: chloroquine; Cys: cysteine; GOT1: glutamic-oxaloacetic transaminase 1, soluble; GPT: glutamic-pyruvic transaminase, soluble; IL1B: interleukin 1 beta; IL6: interleukin 6; KO: knockout; LAMP1: lysosomal associated membrane protein 1; LDH, lactate dehydrogenase; LPS: lipopolysaccharide; LYPLA1: lysophospholipase 1; MAP1LC3/LC3: microtubule associated protein 1 light chain 3; OE: overexpression; qPCR: quantitative polymerase chain reaction; SNAP29: synaptosome associated protein 29; SNARE: soluble N-ethylmaleimide-sensitive factor attachment protein receptor; SQSTM1/p62: sequestosome 1; STX17: syntaxin 17; TNF: tumor necrosis factor; TRIM: tripartite motif-containing; UBA: ubiquitin-associated; UBL: ubiquitin-like; UBQLN: ubiquilin; VAMP8: vesicle associated membrane protein 8; WT: wild-type.

ARTICLE HISTORY

Received 24 September 2022
Revised 27 February 2023
Accepted 24 March 2023






KEYWORDS

Autophagy; CD36; liver injury; ubiquilin 1; proteasomal degradation

Introduction

Sepsis, a condition characterized by systemic hyperinflammation and life-threatening organ dysfunction, causes significant mortality and morbidity worldwide [1]. Liver dysfunction occurs in the early stages of sepsis, and more importantly, it is closely related to the poor prognosis in patients with sepsis [2]. Despite substantial research, the molecular mechanisms of septic liver injury have not been fully elucidated, and thus no effective therapeutic strategies have been established.


CD36 is a widely expressed multifunctional membrane glycoprotein that is important in lipid metabolism, angiogenesis and atherosclerosis. As a member of class B scavenger receptors, CD36 is highly associated with inflammation and CD36 deficiency is the only genetic deficiency state known among scavenger receptors in humans [3]. Global CD36 deficiency reduces peritoneal bacteria counts and improves survival rate, liver and kidney functions in mice by unclear mechanism [4]. Hepatocyte is one of the main hepatic cell types contributing to the liver response during inflammation.

CONTACT Lei Zhao  Zhaolei@cqmu.edu.cn; Xiong Z. Ruan  x.ruan@ucl.ac.uk; Yaxi Chen  chenyaxi@cqmu.edu.cn; Yao Chen  chenyao@cqmu.edu.cn
 Centre for Lipid Research & Chongqing Key Laboratory of Metabolism on Lipid and Glucose, Key Laboratory of Molecular Biology for Infectious Diseases (Ministry of Education), Institute for Viral Hepatitis, Department of Infectious Diseases, the Second Affiliated Hospital, Chongqing Medical University, Chongqing 400016, China

*These authors contributed equally to this work.

#These authors share co-senior authorship.

This article has been corrected with minor changes. These changes do not impact the academic content of the article.

 Supplemental data for this article can be accessed online at <https://doi.org/10.1080/15548627.2023.2196876>.

However, little is known regarding the role of hepatocyte CD36 in septic liver injury.

Autophagy, a process involving the degradation of cytoplasmic constituents, plays a protective role in septic liver injury [5]. Hepatocyte-specific autophagy-deficiency (*atg5* or *atg7* knockout [KO]) exacerbates liver damage and accelerates time to mortality in the murine sepsis model [6,7]. In addition, examination of postmortem liver specimens from septic patients shows an accumulation of autophagic vacuoles in hepatocytes [8]. A significant increased number of autophagosomes and a decreased number of autolysosomes are also observed in livers from septic mice [9]. Many therapeutic agents, such as carbamazepine, dexmedetomidine and genipin are tested to improve septic liver injury in animal models by promoting autophagosome-lysosome fusion [9–11]. These data support that the maintenance of autophagosome-lysosome fusion plays an important protective role in sepsis. In principle, the fusion of autophagosome and lysosome depends on a set of soluble N-ethylmaleimide-sensitive factor attachment protein receptor (SNARE) proteins, of which STX17 (syntaxin 17), the cytosolic SNAP29 (synaptosomal-associated protein 29) and the lysosomal VAMP8 (vesicle-associated membrane protein 8) form a trap core complex mediating fusion [12,13]. Depletion of *STX17* or *SNAP29* or *VAMP8* causes the blockage of autophagosome-lysosome fusion and the accumulation of undigested autophagosome [13].

The ubiquitin-proteasomal system is responsible for regulating a variety of protein functions. However, the cross-talk between the autophagy and ubiquitin-proteasomal pathways remains to be elucidated. UBQLN1 (ubiquilin 1), a member of the UBQLN family, mediates the proteasome targeting of misfolded or accumulated proteins for degradation. Here, we found that CD36 expression was markedly upregulated in hepatocytes from patients with sepsis and septic mouse models, and the hepatocyte-specific *cd36* knockout (*cd36*-HKO) effectively alleviated lipopolysaccharide (LPS)-induced liver injury and autophagosome-lysosome fusion impairment in mice via modulating UBQLN1-mediated proteasomal degradation of autophagic SNARE proteins. These findings not only reveal a new role of CD36 in regulating the proteasomal degradation of autophagic SNARE proteins in a UBQLN1-dependent manner but also suggest that targeting hepatocyte CD36 may represent a new promising approach for the treatment of the septic liver injury.

Results

The expression of CD36 in hepatocytes is elevated in patients and a mouse model with sepsis

To investigate the role of CD36 in sepsis-induced liver injury, we first collected liver samples from humans with or without sepsis. Compared to the non-sepsis controls, the liver tissues of patients with sepsis showed increased inflammatory cell infiltration (Figure 1A). Consistently, inflammatory cell infiltration was higher in the septic livers of C57BL/6J mice than in the normal control livers, accompanied by obviously increased GPT (glutamic – pyruvic transaminase) and GOT1

(glutamic-oxaloacetic transaminase 1) levels in the serum of septic mice (Figure 1B and C). Further analysis showed that the expression of CD36 was increased in hepatocytes from the livers of patients and mice with sepsis (Figure 1D–F).

In vitro, when HepG2 cells were treated with LPS (5 and 10 $\mu\text{g/ml}$) for 24 h, the levels of MAP1LC3/LC3 (microtubule associated protein 1 light chain 3)-II and autophagy substrate SQSTM1/p62 (sequestosome 1) were increased (Figure 1G and H). In L02 cells treated with LPS (2 and 3 $\mu\text{g/ml}$, 24 h), the levels of LC3-II and SQSTM1 were increased compared with control cells (Figure 1G and H). The expression of CD36 protein was also markedly increased in LPS-treated HepG2 (5 and 10 $\mu\text{g/ml}$) and L02 (3 $\mu\text{g/ml}$) cells (Figure 1G and H). Next, HepG2 cells and L02 cells were pretreated with and without the lysosomal inhibitor chloroquine (CQ), followed by LPS for different treatment time (0, 1, 3, 6, 12, 24 h). As shown in Figure S1A–S1C, LPS (10 $\mu\text{g/ml}$ in HepG2 and 3 $\mu\text{g/ml}$ in L02 cells) treatment for 24 h significantly increased the levels of LC3-II and SQSTM1, and CQ could not further increase these two proteins in HepG2 and L02 cells, demonstrating that LPS blocked the late stages of autophagy.

To further support this finding, the mRFP-GFP-LC3 adenovirus was utilized to track the transitions of different stages of the autophagic process. When the autophagosome fuses with lysosome, the green signal from GFP disappears due to the sensitivity of the GFP to acidic conditions. Thus, red-fluorescent puncta and yellow-fluorescent puncta represent autolysosome and autophagosome, respectively. We found fewer numbers of red puncta and more numbers of yellow puncta in LPS-treated cells compared with control cells (Figure 1I–K). This phenomenon could result either from the impaired fusion of autophagosome and lysosome or from elevated lysosomal pH. To distinguish these two possibilities, we next incubated LysoSensor with cells to monitor the acidic condition of lysosome. Our results revealed that the lysosomal acidification was unaltered in the presence of LPS (Figure 1L). Furthermore, the colocalization of endogenous LC3 and LAMP1 (lysosomal associated membrane protein 1) was significantly decreased after LPS treatment in HepG2 cells (Figure 1M). Taken together, these results suggested that a fusion event between autophagosome and lysosome was impaired accompanied with an increase of CD36 expression in hepatocytes stimulated with LPS.

Hepatocyte-specific *cd36* deletion ameliorates LPS-induced liver injury and autophagic flux impairment in mice

To validate the function of hepatic CD36 in the septic liver injury *in vivo*, we generated a *cd36*-HKO mouse strain using the cre-loxP recombination approach and treated them with LPS (12 mg/kg) to induce sepsis. Histopathology of liver sections demonstrated that *cd36*-HKO mice had improved liver histology, with significantly fewer numbers of infiltrated inflammatory cells and apoptotic cells, compared to *Cd36*^{fllox/fllox} mice (Figure 2A). The serum GPT and GOT1 contents and hepatic LDH (lactate dehydrogenase) activity were significantly decreased in *cd36*-HKO mice compared to *Cd36*^{fllox/fllox} mice (Figure 2B). Meanwhile, *cd36* deficiency decreased

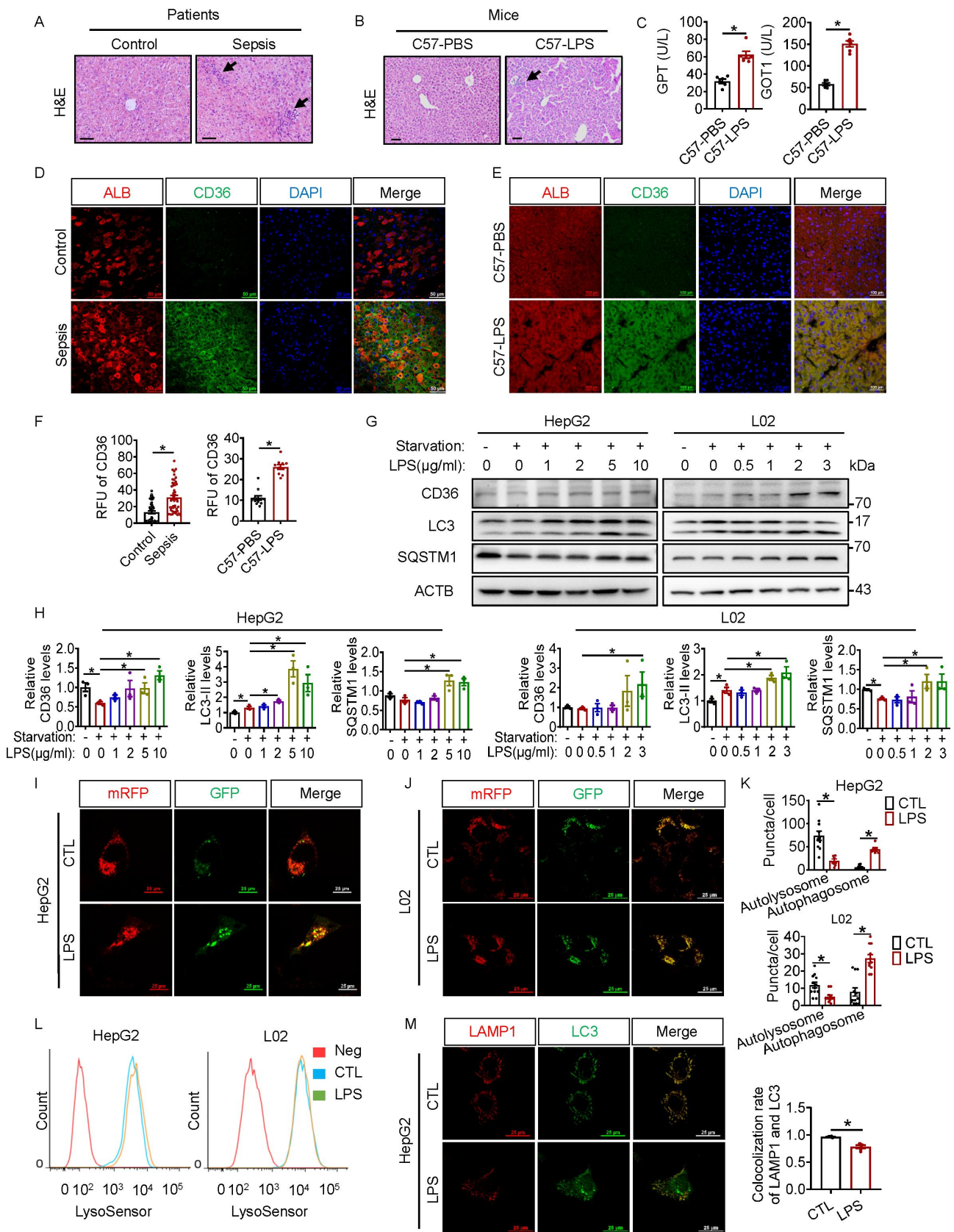


Figure 1. The expression of CD36 in hepatocytes is elevated in patients and mouse models with sepsis. **(A)** H&E staining of liver sections from individuals with or without sepsis. $n = 6$ per group. Arrows pointed at the inflammatory cells. Scale bars: 50 μ m. **(B)** H&E staining of liver sections from C57BL/6J mice with or without LPS injection. $n = 6$ per group. Arrows pointed at the inflammatory cells. Scale bars: 50 μ m. C57, C57BL/6J. **(C)** Serum GPT and GOT1 levels of C57BL/6J mice 12 h after injection with LPS. **(D)** Confocal microscopy images of ALB (albumin; red) and CD36 (green) in liver samples from patients with or without sepsis. Scale bars: 50 μ m. **(E)** Confocal microscopy images of ALB (red) and CD36 (green) in liver sections of mice with or without LPS injection. Scale bars: 100 μ m. **(F)** The levels of relative fluorescence unit (RFU) for CD36 in liver sections were analyzed by ImageJ software. **(G, H)** HepG2 and L02 cells were treated with or without different concentrations of LPS for 24 h. The protein levels of CD36, SQSTM1 and LC3-II were measured by western blotting **(G)**. The bands were calculated by ImageJ software **(H)**. **(I-K)**

the mRNA levels of hepatic inflammatory cytokines, including *Il1b* (interleukin 1 beta), *Il6* (interleukin 6), *Tnf* (tumor necrosis factor) and *Ccl2* (chemokine [C-C motif] ligand 2) (Figure 2C). Meanwhile, the protein levels of inflammatory cytokines (IL1B, IL6 and TNF) and apoptotic markers (cleaved-CASP3 [caspase 3] and cleaved-CASP8 [caspase 8]) were increased in livers of *Cd36^{flox/flox}* mice with LPS injection compared with *Cd36^{flox/flox}* mice with PBS injection, while these protein levels were significantly decreased in livers of *cd36*-HKO mice compared with *Cd36^{flox/flox}* mice in the presence of LPS (Figure 2D and E). Since insufficient autophagic flux is associated with the pathogenesis of septic acute liver injury, we next investigated whether *cd36* deficiency influenced autophagy flux in sepsis. We found that LPS increased the levels of SQSTM1 and LC3-II in *Cd36^{flox/flox}* mice (Figure 2D and E). In the presence of LPS, the SQSTM1 levels were decreased and the LC3-II levels were increased in *cd36*-HKO mice livers when compared with *Cd36^{flox/flox}* mice livers (Figure 2D and E). Consistently, the number of LC3 puncta was increased in *cd36*-HKO mice livers with LPS injection compared to *Cd36^{flox/flox}* mice livers with LPS (Figure 2F). Transmission electron microscopy showed that the number of autolysosomes (indicated by arrows) was decreased in *Cd36^{flox/flox}* mice after LPS injection while *cd36*-HKO increased the number of autolysosomes in the presence of LPS (Figure 2G). These data indicated that *cd36*-HKO alleviated LPS-induced fusion impairment of autophagosome with lysosome and acute liver injury in mice.

CD36 regulates the fusion of the autophagosome with lysosome in LPS-treated hepatocytes

We next constructed *CD36* KO HepG2 and L02 cell lines using the CRISPR-Cas9 approach, as well as *CD36* overexpression (*CD36* OE) cell lines with the lentivirus vectors expressing wild-type (WT)-*CD36* (Figure S2A). These cells were treated with LPS to validate the role of *CD36* in modulating autophagy during sepsis. Compared with respective control cells, the protein levels of SQSTM1 and cleaved-CASP3 were decreased and the LC3-II levels were increased in *CD36* KO cells in the presence of LPS (Figure 3A). In LPS-treated *CD36* OE HepG2 and L02 cells, the levels of LC3-II, SQSTM1 and cleaved-CASP3 were elevated compared to respective control cells (Figure 3B). Moreover, *CD36* KO significantly decreased the number of yellow-fluorescent puncta (autophagosome) and increased the number of red-fluorescent puncta (autolysosome) in HepG2 and L02 cells (Figure 3C), while the number of yellow-fluorescent puncta was increased and the number of red-fluorescent puncta was decreased upon *CD36* OE (Figure 3D). Notably, *CD36* OE or KO did not change the lysosomal pH in the presence of LPS

(Figure 3E). In addition, in the presence of LPS, the colocalization rate of LAMP1 and LC3 was substantially enhanced by nearly 20% in *CD36* KO cells compared with the control cells (con), while *CD36* OE cells exhibited nearly 25% reduction in colocalization rate of LAMP1 and LC3 related to cells infected with negative control vector (NC) (Figure 3F and G). Transmission electron microscopy also showed that the number of autolysosomes (indicated by arrows) was decreased in *CD36* OE cells while *CD36* KO increased the number of autolysosomes in cells (Figure 3H).

We also conducted two independent clonal *CD36* KO cell lines using two different sgRNA sequences and rescued *CD36* expression in these *CD36* KO cells using lentiviral vector carrying WT-*CD36* cDNA (Figure S2B). The *CD36* KO cell lines and the rescued KO cell lines were treated with and without the lysosomal inhibitor CQ in the presence of LPS. In the absence of CQ, these two different sgRNA for knocking out *CD36* increased LC3-II levels and decreased SQSTM1 levels. CQ treatment increased the levels of LC3-II and SQSTM1 in *CD36* KO cells (Figure S2C-S2E). Notably, compared with *CD36* KO cell lines, the levels of LC3-II and SQSTM1 were increased in the rescued KO cell lines without CQ treatment, and there was no obvious difference in LC3-II and SQSTM1 levels between the rescued KO lines with or without CQ treatment, supporting that *CD36* OE impaired the fusion of lysosome with autophagosome (Figure S2C-S2E). In addition, the immunofluorescent staining of LC3 puncta was consistent with the above results of western blotting (Figure S3A). The two sgRNAs targeting *CD36* also significantly increased the number of red-fluorescent puncta (autolysosome) and decreased the number of yellow-fluorescent puncta (autophagosome), while the number of red-fluorescent puncta was decreased and the number of yellow-fluorescent puncta was increased in the rescued cells compared with KO cells (Figure S3B). Taken together, these results strongly suggested that *CD36* played a key role in the regulation of the fusion of autophagosome with lysosome in hepatocytes.

CD36 regulates the proteasomal degradation of autophagic SNARE proteins in LPS-treated hepatocytes

To further explore the underlying mechanism of *CD36* regulating autophagosome-lysosome fusion, we examined whether *CD36* affected the formation of autophagic SNARE complex (STX17-SNAP29-VAMP8), which has been recognized as the key factor in mediating autophagosome-lysosome fusion. Co-immunoprecipitation (co-IP) showed that *CD36* OE decreased the formation of STX17-SNAP29-VAMP8 complex upon LPS stimulus, while *CD36* KO increased this complex formation (Figure 4A and B). Next,

HepG2 and L02 cells were transfected with mRFP-GFP-LC3 and treated with or without LPS (10 µg/ml in HepG2 and 3 µg/ml in L02) for 24 h. Representative confocal images of mRFP-GFP-LC3 in HepG2 (I) and in L02 cells (J). Scale bars: 25 µm. The autophagosome and autolysosome number in HepG2 and L02 cells was quantified by ImageJ software (K). CTL, control. (L) Cells were pretreated with LPS (10 µg/ml in HepG2 and 3 µg/ml in L02) for 24 h, then incubated with 0.1 µM LysoSensor Green DND-189 for 30 min, fluorescent spot counts were determined by flow cytometry. Neg, negative control. (M) Representative confocal images and colocalization rate of LC3 (green) and LAMP1 (red) in HepG2 cells treated with or without LPS (10 µg/ml) for 24 h. Scale bars: 25 µm. For G to L, $n = 3$ independent experiments. * $P < 0.05$. All data were shown as the mean \pm SEM.

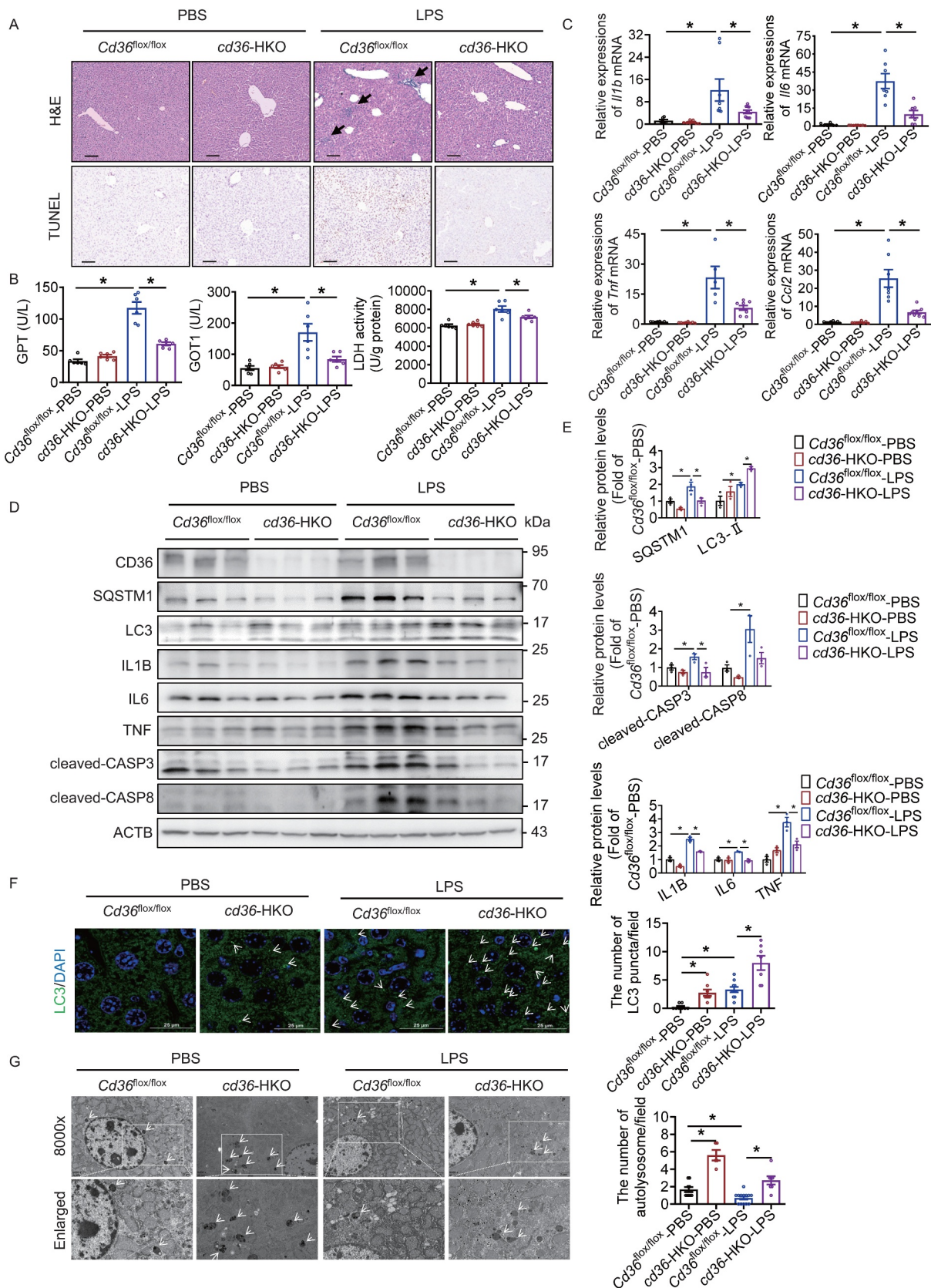


Figure 2. *Cd36*-HKO ameliorates LPS-induced liver injury and autophagic flux impairment in mice. **(A)** H&E and TUNEL staining of liver sections from *Cd36*^{fllox/fllox} and *cd36*-HKO mice with or without LPS injection. $n = 6$ per group. Scale bars: 100 μ m. Arrows pointed at the inflammatory cells. **(B)** Serum GPT and GOT1 levels and hepatic LDH activity of *Cd36*^{fllox/fllox} and *cd36*-HKO mice after 12 h injection with LPS. **(C)** The mRNA expression of *Il1b*, *Il6*, *Tnf* and *Ccl2* in livers from *Cd36*^{fllox/fllox} and *cd36*-HKO mice with or without LPS injection was analyzed by q. **(D, E)** The protein levels of CD36, SQSTM1, LC3-II, IL1B, IL6, TNF, cleaved-CASP3 and cleaved-CASP8 in livers from *Cd36*^{fllox/fllox} and *cd36*-HKO mice with or without LPS injection were measured by western blotting (D). The bands were quantified using Image J software (E). **(F)** Representative immunofluorescent images and quantification of LC3 puncta in livers from *Cd36*^{fllox/fllox} and *cd36*-HKO mice with or without LPS injection. Arrows indicated the LC3 puncta. **(G)** Representative electronic microscope graphs and quantification of autolysosome numbers in livers from *Cd36*^{fllox/fllox} and *cd36*-HKO mice with or without LPS injection. Scale bars: 2 μ m. Arrows indicated the autolysosome. * $P < 0.05$. All data were shown as the mean \pm SEM.

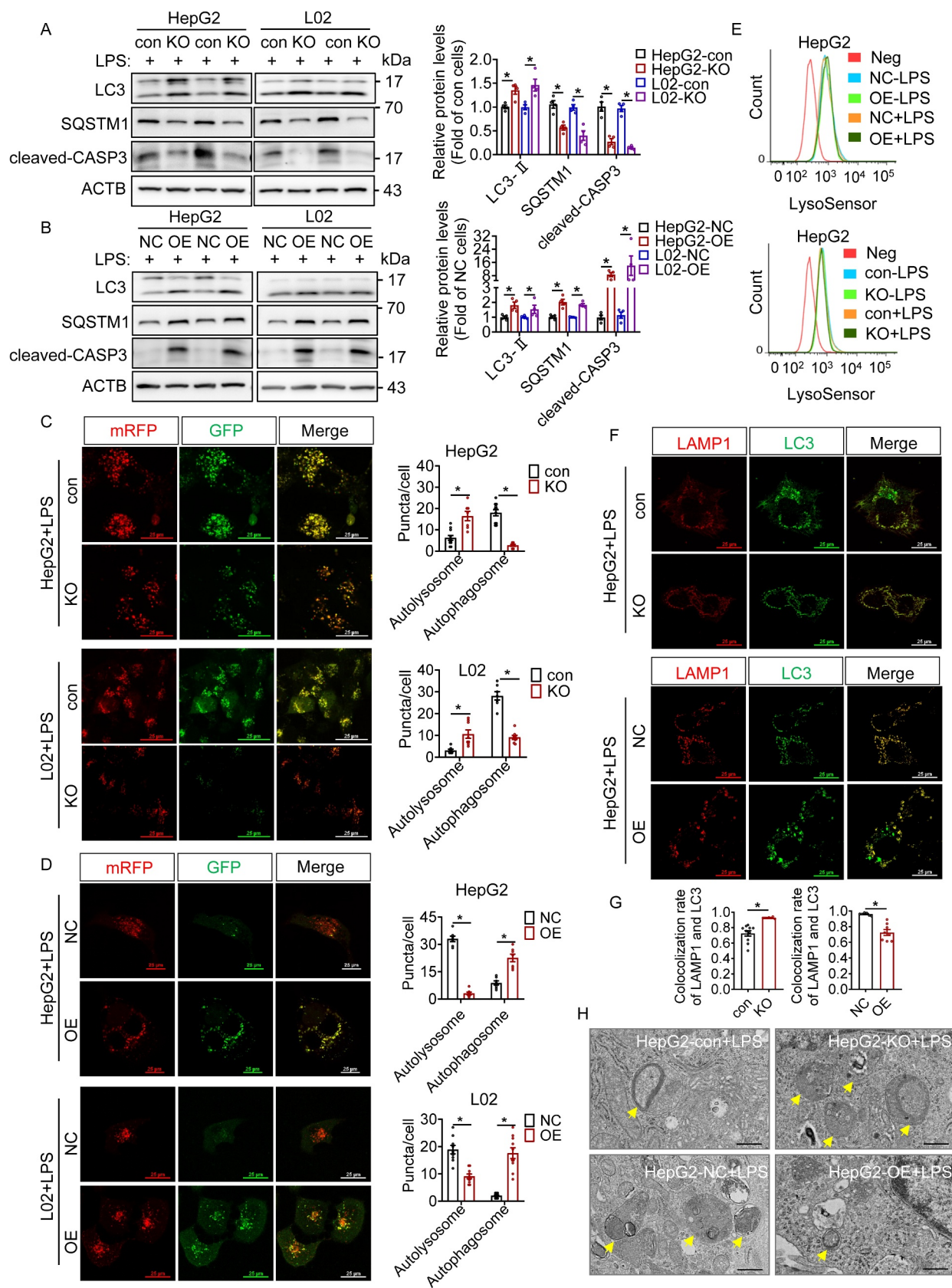


Figure 3. CD36 regulates the fusion of the autophagosome with lysosome in LPS-treated hepatocytes. **(A)** Western blot analysis of SQSTM1 and LC3-II protein levels in CD36 KO cells treated with LPS (10 μ g/ml in HepG2 and 3 μ g/ml in L02) for 24 h. **(B)** Western blot analysis of SQSTM1 and LC3-II protein levels in CD36 OE cells treated with LPS (5 μ g/ml in HepG2 and 2 μ g/ml in L02) for 24 h. **(C)** Representative confocal images and quantification of autophagosome and autolysosome numbers in CD36 KO cells transduced with mRFP-GFP-LC3 followed by LPS (10 μ g/ml in HepG2 and 3 μ g/ml in L02) treatment for 24 h. Scale bars: 25 μ m. **(D)** Representative confocal images and quantification of autophagosome and autolysosome numbers in CD36 OE cells transduced with mRFP-GFP-LC3 followed by LPS treatment (5 μ g/ml in HepG2 and 2 μ g/ml in L02) for 24 h. Scale bars: 25 μ m. **(E)** Cells were incubated with 0.1 μ M LysoSensor Green DND-189 for 30 min, fluorescent spot counts were determined by flow cytometry. **(F, G)** Representative confocal microscopy images (F) and colocalization rate (G) of LC3 (green) and LAMP1 (red) in HepG2 cells treated with LPS (10 μ g/ml in CD36 KO cells and 5 μ g/ml in CD36 OE cells) for 24 h. Scale bars: 25 μ m. **(H)** Transmission electron microscope images of HepG2 cells with LPS (10 μ g/ml in CD36 KO cells and 5 μ g/ml in CD36 OE cells) treatment. The arrows indicated the autolysosome. Scale bars: 500 nm. All results were performed at least 3 independent experiments. * $P < 0.05$. All data were shown as the mean \pm SEM.

we performed quantitative polymerase chain reaction (qPCR) to detect the mRNA levels of *STX17*, *SNAP29* and *VAMP8* in *CD36* KO and OE HepG2 cells and found that the expression of mRNA encoding these proteins was unaltered relative to respective control cells (Figure S4). Interestingly, treatment with LPS reduced the protein expression of *SNAP29* and *VAMP8* in HepG2 cells versus control HepG2 cells (Figure 4C). *CD36* KO increased the protein levels of *SNAP29* and *VAMP8* in the presence of LPS, while *CD36* OE obviously decreased these two protein levels (Figure 4C). We also observed that the modulation of *CD36* expression (KO and OE) did not affect the protein expression of *STX17* in hepatocytes (Figure 4C). These results suggested that regulating *SNAP29* and *VAMP8* by *CD36* involved a post-transcriptional mechanism.

Ubiquitin-proteasome pathway is one of the most common post-transcriptional mechanisms for regulating protein expression. We treated *CD36* OE cells with proteasome inhibitor MG132 and found that the decrease of *SNAP29* and *VAMP8* proteins in *CD36* OE cells were recovered by MG132 incubation, indicating a proteasome-dependent mechanism of *CD36*-regulated *SNAP29* and *VAMP8* degradation (Figure 4D). Moreover, we found that *CD36* KO promoted the stability of *SNAP29* and *VAMP8* proteins in HepG2 cells (Figure 4E and F). Accordingly, the stability of *SNAP29* and *VAMP8* proteins was significantly decreased in *CD36* OE cells relative to control cells (Figure 4E and F). Ubiquitination experiments further showed that *CD36* KO significantly decreased the ubiquitination of endogenous *SNAP29* and *VAMP8* (Figure 4G and H), while *CD36* OE increased the ubiquitination of *SNAP29* and *VAMP8* proteins in HepG2 cells (Figure 4G and H). Together, these results suggested that *CD36* was important in the modulation of ubiquitin-proteasome degradation of *SNAP29* and *VAMP8* proteins.

UBQLN1 plays a key role in CD36 regulation of SNARE proteins in hepatocytes

To further explore the specific molecular mechanism of *CD36* regulating the ubiquitin-proteasome degradation of *SNAP29* and *VAMP8* proteins, we screened for the candidate target proteins of *CD36* in HepG2 cells using co-IP followed by LC-MS/MS (Figure 5A and Data S1-S2). Three proteins involved in the ubiquitin-proteasome system, including TRIM25 (tripartite motif-containing 25), TRIM38 (tripartite motif-containing 38) and *UBQLN1*, were identified as potential candidates. We found that knocking down of *UBQLN1* showed the most obvious improvement effect on *CD36* OE-induced autophagy flux blockage among all candidate proteins (Figure 5B). *UBQLN1* is a primarily cytosolic protein, and its ubiquitin-associated (UBA) domain binds to poly-ubiquitin chains of substrate and shuttles it to the proteasome via its ubiquitin-like (UBL) domain for degradation (Figure 5C). To verify the key role of *UBQLN1* in *CD36*-regulated autophagosome and lysosome fusion, the *UBQLN1* small interfering RNA (siRNA) and the plasmid vector containing *UBQLN1* cDNA were employed in *CD36* OE and KO cell model, respectively. We found that the protein expression of *SNAP29*

and *VAMP8* was decreased in *CD36* KO cells transfected with *UBQLN1* OE plasmid compared to *CD36* KO cells transfected with empty vector (Figure 5D). When *UBQLN1* was knocked down, the inhibitory effect of *CD36* OE on *SNAP29* and *VAMP8* proteins expression was also reversed (Figure 5D). Meanwhile, knocking down of *UBQLN1* inhibited the accumulation of *SQSTM1* induced by *CD36* OE, while *UBQLN1* OE increased the expression of *SQSTM1* in *CD36* KO cells (Figure 5D). Using the mRFP-GFP-LC3 reporter, we next investigated the impact of *UBQLN1* on autophagic flux in *CD36* OE and KO cells. Compared with control cells, *UBQLN1* OE inhibited the promotion effects of *CD36* KO on autophagy flux (Figure 5E) and knockdown of *UBQLN1* prevented the inhibition of autophagic flux by *CD36* OE (Figure 5F). These data suggested that *CD36* regulated the SNARE-mediated fusion of autophagosome and lysosome in a *UBQLN1*-dependent manner.

We next explored how *CD36* regulated *SNAP29* and *VAMP8* through *UBQLN1*. The co-IP assays showed that *CD36* could bind to *UBQLN1*, *SNAP29* and *VAMP8* proteins (Figure 5G). In addition, *CD36* OE promoted the interaction between *UBQLN1* and the autophagic SNARE proteins, while *CD36* KO decreased the binding between *UBQLN1* and the autophagic SNARE proteins (Figure 5H), suggesting that *CD36* might mediate the ubiquitin-proteasome proteolytic pathway of autophagic SNARE proteins by facilitating the binding of *UBQLN1* to *SNAP29* and *VAMP8*.

Hepatic Ubqln1 OE blocks the protective effect of cd36-HKO on LPS-induced liver injury in mice

To investigate the role of *UBQLN1* in septic liver injury of *cd36*-HKO mice, adeno-associated virus 8 (AAV8) vectors were used to overexpress *Ubqln1* in *cd36*-HKO and *Cd36^{fllox/fllox}* mice (Figure 6A). Compared with *cd36*-HKO mice with control vectors, *cd36*-HKO mice with *Ubqln1* OE vectors were at risk of increased inflammation and apoptosis (Figure 6B), as well as increased levels of serum GPT and GOT1 and hepatic LDH activity (Figure 6C). Higher mRNA levels of inflammatory cytokines (*Il1b*, *Il6*, *Tnf* and *Ccl2*) were observed in the liver of *cd36*-HKO mice after being injected with AAV8-*Ubqln1* (Figure 6D). Consistently, *Ubqln1* OE increased the protein levels of inflammatory cytokines (IL1B, IL6 and TNF) and apoptotic markers (cleaved-CASP3 and cleaved-CASP8) in *cd36*-HKO mice livers after LPS injection (Figure 6E and F). Moreover, compared with *Cd36^{fllox/fllox}* mice with control vectors, the LC3-II levels were increased and the *SQSTM1* levels were decreased in the liver of *cd36*-HKO mice with control vectors, accompanied by an increase in *SNAP29* and *VAMP8* protein levels (Figure 6E and F). Notably, *cd36*-HKO mice transduced with AAV8-*Ubqln1* displayed increased levels of *SQSTM1* and LC3-II and decreased protein expression of *SNAP29* and *VAMP8* in the livers (Figure 6E and F). Taken together, our results suggested that *Ubqln1* OE in *cd36*-HKO mice aggravated LPS-induced septic liver injury by blocking autophagic flux.

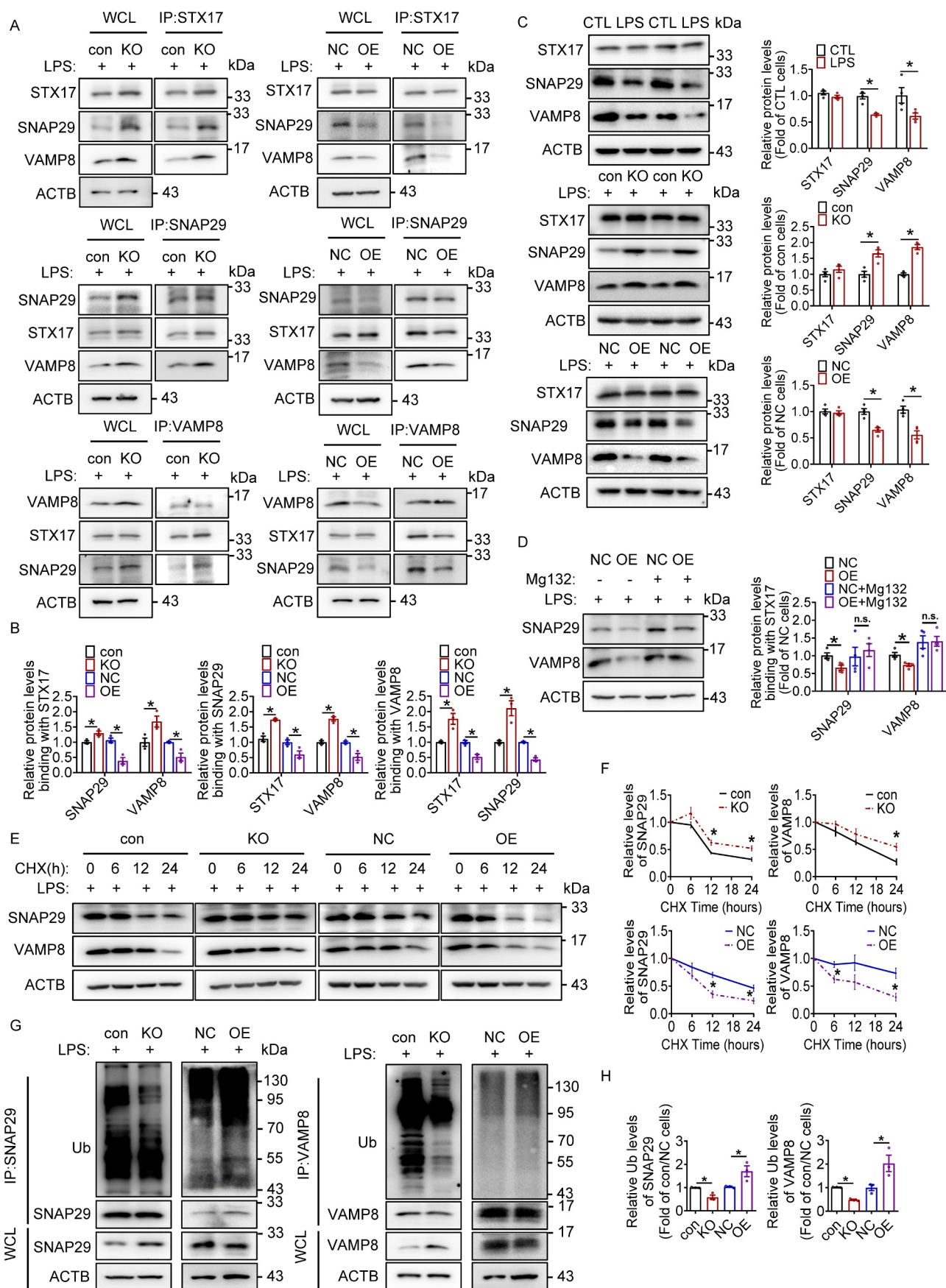


Figure 4. CD36 regulates the proteasomal degradation of autophagic SNARE proteins in LPS-treated hepatocytes. **(A, B)** The formation of SNAP29-STX17-VAMP8 complex in HepG2 cells with LPS treatment (10 μ g/ml in CD36 KO cells and 5 μ g/ml in CD36 OE cells) was measured using co-IP (A) and the bands were quantified by Image J software (B). WCL, whole cell lysis. **(C)** Western blot analysis of STX17, SNAP29 and VAMP8 protein levels in HepG2 cells with or without LPS treatment. **(D)** NC and OE HepG2 cells were pretreated with LPS (5 μ g/ml) for 24 h, followed by MG132 (3 μ M) for 12 h before harvested, and then the protein expression of SNAP29

Palmitoylation of CD36 is important for CD36-UBQLN1-SNARE complex formation

As shown in Figure 5G, there is an interaction between CD36 with UBQLN1, SNAP29 and VAMP8 proteins. Further study showed that this interaction was enhanced under LPS treatment (Figure 7A). Considering that CD36 is mainly expressed on the plasma membrane under physiological conditions, we speculated that LPS might induce the internalization of CD36. Since the palmitoylation of CD36 is required for its plasma membrane localization [14], we first examined the palmitoylation of CD36 using IP and acyl-biotin exchange, and found that the palmitoylated CD36 protein was significantly decreased in CD36 OE cells treated with LPS compared to CD36 OE cells without LPS treatment (Figure 7B).

Previous studies have reported that LYPLA1 (lysophospholipase 1) is the depalmitoylase of CD36 [15]. We then examined whether blocking depalmitoylation of CD36 by inhibiting LYPLA1 would affect LPS-modulated the internalization of CD36. We treated HepG2 cells with ML348 (a selective inhibitor of LYPLA1) and checked the colocalization of CD36 with ATP1A1 (ATPase, Na⁺/K⁺ transporting, alpha 1 polypeptide, a plasma membrane marker). As shown in Figure 7C and G, LPS treatment significantly decreased CD36 distribution in the plasma membrane, while this effect was blocked in cells treated with ML348, indicating that depalmitoylation of CD36 was required for LPS-mediated internalization of CD36. We then examined the effect of palmitoylation on the subcellular localization of CD36 using a CD36 mutant (CD36[AA-SS]) that the palmitoylation sites cysteines (Cys3, 7) of CD36 were replaced with alanine, and the residues toward the carboxyl terminus (Cys464, 466) were replaced with serine. Indeed, CD36[AA-SS] significantly decreased the plasma membrane localization of CD36 in the absence of LPS (Figure 7D and G). In addition, we examined the colocalization of CD36 with endosome/lysosome and autophagosome. As shown in Figure S5, we barely observed colocalization of CD36 with LC3 (autophagosome marker) in the presence of LPS. Notably, the colocalization of CD36 with RAB5 (endosome marker) and LAMP1 (lysosome marker) was enhanced by LPS, suggesting that LPS promoted CD36 endocytosis and its distribution in lysosome (Figure 7E-G). In the absence of LPS, there were more colocalization of CD36[AA-SS] protein with RAB5 and LAMP1 than WT-CD36 with RAB5 and LAMP1 (Figure 7E-G). Moreover, the formation of the CD36-UBQLN1-SNARE complex was increased when the palmitoylation sites of CD36 were mutated (Figure 7H). The protein levels of SNAP29 and VAMP8 were also downregulated in CD36[AA-SS] cells without LPS treatment (Figure 7I). These findings strongly supported that LPS promoted the endocytosis of CD36 by

increasing its depalmitoylation, and then CD36 was distributed to the lysosomal membrane to recruit UBQLN1 and SNARE proteins, and hence regulating the fusion of autophagosome with autolysosome.

The working model (Figure 7J) depicts how CD36 regulated septic liver injury. In response to sepsis, hepatocytes CD36 got depalmitoylated and translocated from the plasma membrane to the lysosome. CD36 then recruited UBQLN1 to promote the degradation of the autophagic SNARE proteins, contributing to fusion impairment and septic liver injury. CD36 deletion in hepatocytes blocked the formation of CD36-UBQLN1-SNARE complex and hence improving acute liver injury during sepsis.

Discussion

Sepsis-induced acute liver injury is a potentially life-threatening condition, and new effective therapies are needed to improve liver function during sepsis.

In the process of sepsis, autophagy is a critical defense mechanism and is expected to become a promising therapeutic target [11]. Classical autophagy begins with the capture of unnecessary material into autophagosome, which is followed by the fusion of autophagosome with lysosome to generate the autolysosome, allowing lysosomal hydrolases to break down the contents within this organelle [16]. Our data showed that LPS could impair the fusion of autophagosome and lysosome in hepatocytes. *In vivo*, *cd36*-HKO ameliorated LPS-induced fusion impairment and liver injury in mice. *In vitro*, CD36 OE aggravated the impairment of autophagosome-lysosome fusion induced by LPS, while CD36 KO attenuated this fusion impairment in hepatocytes.

A major event during autophagosome-lysosome fusion is the formation of the autophagic SNARE complex. SNARE proteins are divided into four sub-families: Qa-, Qb-, Qc-, and R-SNARE. Autophagosome-localized STX17 (Qa), SNAP29 (Qbc), and lysosome-localized VAMP8 (R) assemble into the autophagic SNARE complex, mediating the fusion of autophagosome and lysosome. In the present study, we identified CD36 as an essential regulator of the autophagic SNARE complex as it facilitated the ubiquitin-proteasome degradation of SNAP29 and VAMP8 proteins.

In *Drosophila* fat bodies, *snap29* depletion results in complete inhibition of starvation-induced autolysosome formation as well as in accumulation of ATG8-positive autophagosome, indicating a key role for SNAP29 in autophagy flux and autophagosome-lysosome fusion [17]. The alteration of SNAP29 is highly associated to human disease such as schizophrenia and virus infection [18]. VAMP8 has also been reported to be essential for chemical and infectious colitis [19], virus infection [20], and lung cancer [21]. Here we provided further evidence supporting that SNAP29 and

and VAMP8 was detected by western blotting and analyzed by Image J software. (E, F) HepG2 cells were incubated with 200 µg/mL cycloheximide (CHX) and LPS (10 µg/ml in CD36 KO cells and 5 µg/ml in CD36 OE cells) and then harvested at the indicated times. The protein levels of SNAP29 and VAMP8 were examined by western blotting (E) and quantified (F) using Image J software. (G, H) Ubiquitination (Ub) levels of SNAP29 and VAMP8 in HepG2 cells in response to LPS (10 µg/ml in CD36 KO cells and 5 µg/ml in CD36 OE cells) treatment were measured by co-IP (G) and the bands were quantified by Image J software (H). All results were performed at least 3 independent experiments. *P < 0.05, and n.s. indicated no significance between the two indicated groups. All data were shown as the mean ± SEM.

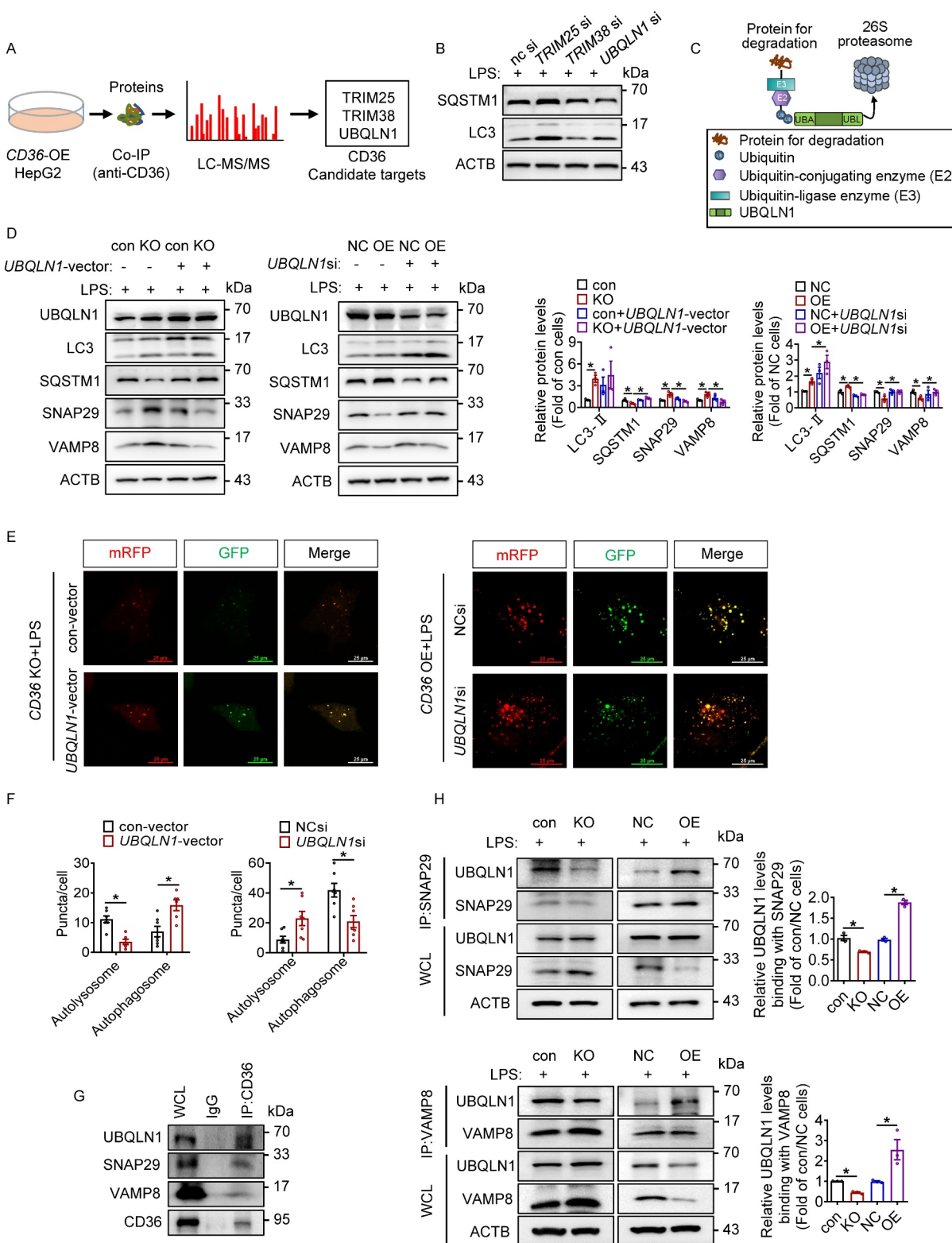


Figure 5. UBQLN1 plays a key role in CD36 regulation of SNARE proteins in hepatocytes. **(A)** The schematic showed the process of exploring for CD36 candidate targets. Using mass spectrometry based on co-IP of CD36 in CD36 OE HepG2 cells with or without LPS treatment (5 µg/ml). **(B)** The representative western blot showed the effect of *TRIM25*, *TRIM38* and *UBQLN1* knockdown on the protein expression of SQSTM1 and LC3-II in CD36 OE HepG2 cells with LPS treatment (5 µg/ml). **(C)** UBQLN1 targets ubiquitinated substrates and drives substrates degradation by the 26S proteasome. UBA, ubiquitin-associated domain, UBL, ubiquitin-like domain. **(D)** The effects of *UBQLN1* OE and knockdown on LC3-II, SQSTM1, SNAP29 and VAMP8 protein levels in CD36 KO and OE HepG2 cells in the presence of LPS (10 µg/ml in CD36 KO cells and 5 µg/ml in CD36 OE cells) were measured by western blotting analysis. **(E, F)** Representative confocal images of mRFP-GFP-LC3 in HepG2 cells transfected with *UBQLN1* vector or *UBQLN1* siRNA in the presence of LPS (10 µg/ml in CD36 KO cells and 5 µg/ml in CD36 OE cells) (E). The number of autophagosome and autolysosome per cell was analyzed by Image J software (F). **(G)** The interaction of CD36 with UBQLN1, SNAP29 and VAMP8 in CD36 OE HepG2 cells with LPS treatment (5 µg/ml) was measured by co-IP. **(H)** The interaction of UBQLN1 with SNAP29 and VAMP8 in HepG2 cells with LPS treatment (10 µg/ml in CD36 KO cells and 5 µg/ml in CD36 OE cells) was analyzed by co-IP. All results were performed at least 3 independent experiments. **P* < 0.05. All data were shown as the mean ± SEM.

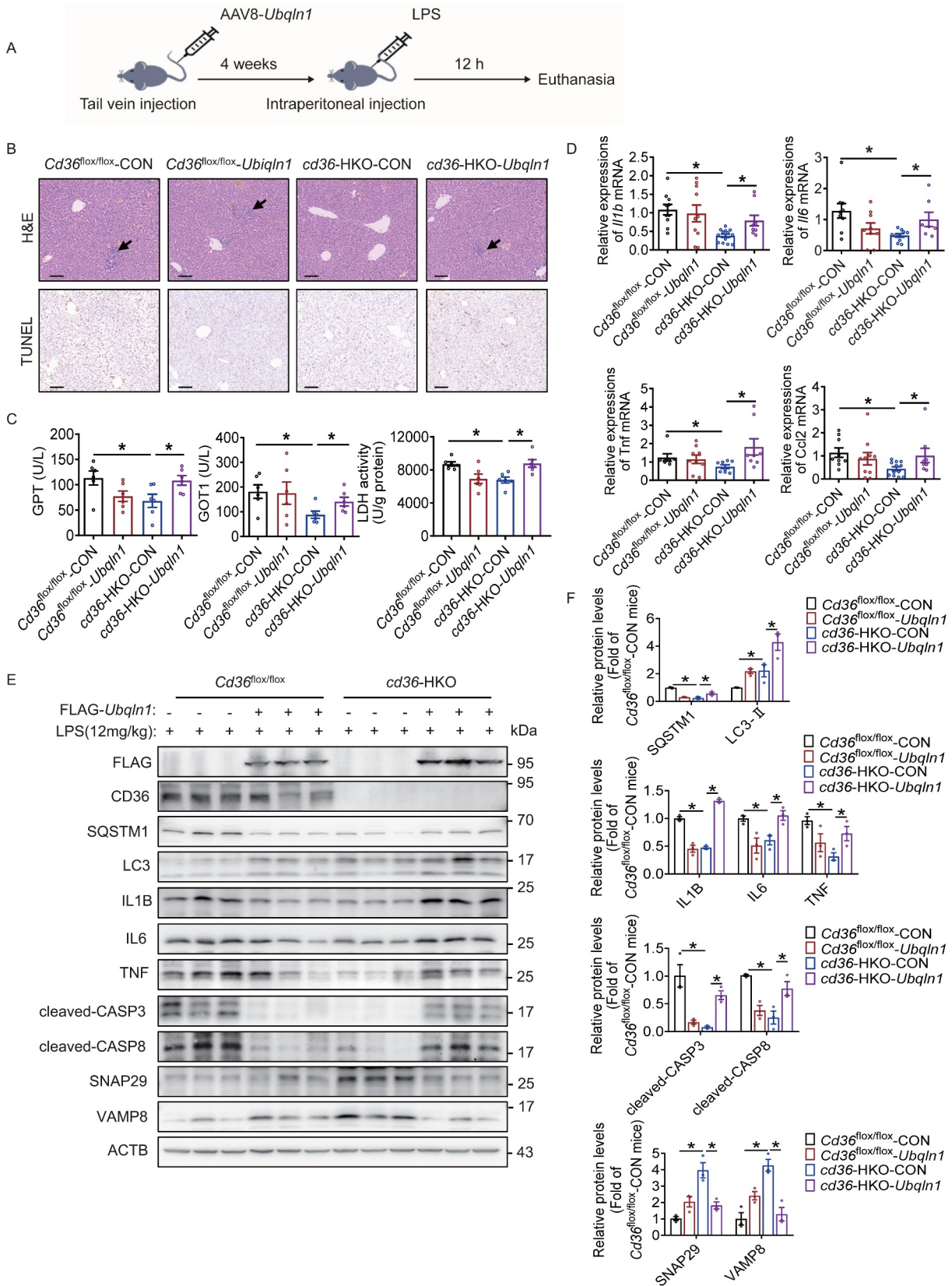
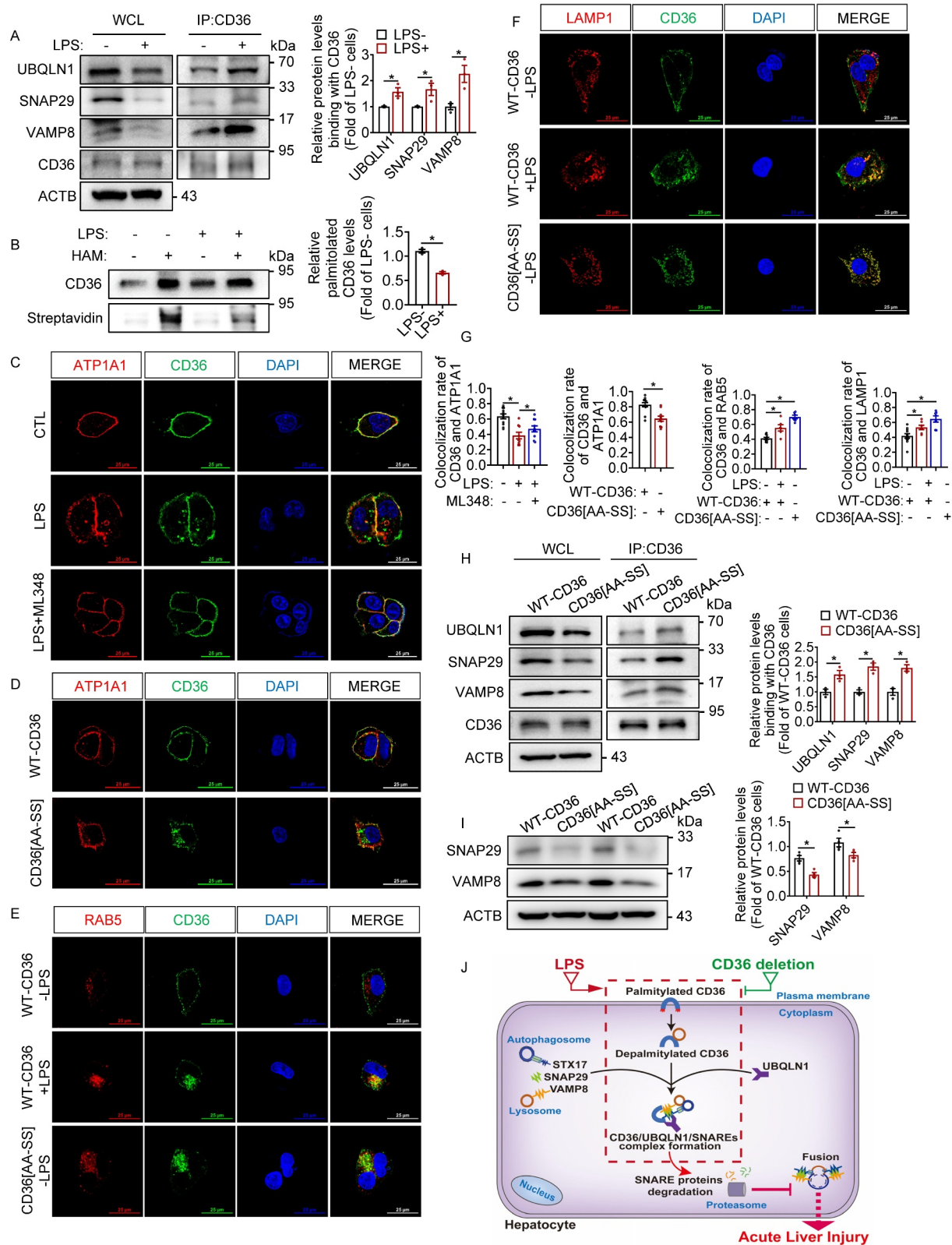


Figure 6. Hepatic *Ubqln1* OE blocks the protective effect of *cd36*-HKO on LPS-induced liver injury in mice. **(A)** *Cd36*^{flox/flox} and *cd36*-HKO mice aged 8 to 10 weeks were injected with AAV8-*Apoe-Ubqln1* or AAV8-*Apoe*-null by tail vein. After 4 weeks, mice were injected intraperitoneally with LPS at a dosage of 12 mg/kg body weight for 12 h. **(B)** Representative images of H&E and TUNEL staining of liver tissues in different groups. *n* = 6 per group. Scale bars: 100 μ m. Arrows pointed at the inflammatory cells. **(C)** Serum GPT and GOT1 levels and hepatic LDH activity of *Cd36*^{flox/flox} and *cd36*-HKO mice with or without *Ubqln1* OE. **(D)** The mRNA expression of *Il1b*, *Il6*, *Tnf* and *Ccl2* in livers from *Cd36*^{flox/flox} and *cd36*-HKO mice with or without *Ubqln1* OE was analyzed by qPCR. **(E, F)** Western blot analysis of FLAG/UBQLN1, CD36, SQSTM1, LC3-II, IL1B, IL6, TNF, cleaved-CASP3, cleaved-CASP8, SNAP29 and VAMP8 protein levels in livers from *Cd36*^{flox/flox} and *cd36*-HKO mice with or without *Ubqln1* OE (E). The bands were quantified by Image J software (F). **P* < 0.05. All data were shown as the mean \pm SEM.



VAMP8 might contribute to acute liver injury via modulating autophagosome-lysosome fusion during sepsis.

The ubiquitin-proteasome system has emerged as an attractive therapeutic target for human diseases. Previous studies have supported the critical functions of numerous ubiquitin ligases in liver injury [22]. In this study, we screened and confirmed that CD36 was a key linking molecule binding to both the autophagic SNARE proteins and UBQLN1. Furthermore, the regulation of CD36 on the proteasomal degradation of autophagic SNARE proteins was dependent on UBQLN1. Although STX17 also could bind to UBQLN1 and CD36, the protein stability of STX17 was not regulated by CD36, which might be related to the more stable expression of STX17 protein (Data were not shown).

UBQLN1, a member of UBQLN family, is recognized as a shuttle protein by delivering poly-ubiquitinated proteins to the proteasome for degradation. The limited studies showed that UBQLN1 regulates autophagy with unclear mechanisms [23–25]. In human neuronal cells, Şentürk et al. reported that *UBQLN1* loss leads to decreased mammalian target of rapamycin signaling, and hence upregulating autophagic flux [23]. However, *UBQLN1* OE enhances starvation-induced autophagy in HeLa cells [24]. In the present study, we found that hepatocyte *Ubqln1* OE blocked the protective effect of *cd36*-HKO on LPS-induced liver injury and autophagic flux blockage in mice, while *Ubqln1* OE improved liver injury and autophagy impairment in *Cd36^{flox/flox}* mice livers. It seems that the role of UBQLN1 in autophagy is complex. UBQLN1 may regulate autophagy via different mechanisms under different backgrounds.

Furthermore, we have identified a critical role of CD36 palmitoylation in regulating the proteasomal degradation of SNARE proteins. It's well known that protein palmitoylation is required for the plasma membrane localization of CD36 [14,26]. On the plasma membrane, ZDHHC5 (zinc finger DHHC-type palmitoyltransferase 5) maintains the cell-surface localization of CD36 by protecting it from depalmitoylation [27]. In this study, LPS treatment promoted CD36 translocation from the plasma membrane to the lysosome by increasing CD36 depalmitoylation, and hence enhancing the formation of CD36-UBQLN1-SNAREs complex. In addition, compared with cells expressing WT-CD36, cells expressing CD36[AA-SS] showed increased CD36 distribution from the plasma membrane to the endosome/lysosome and the formation of CD36-UBQLN1-SNAREs complex in the absence of LPS. Consistently, the lack of CD36 palmitoylation down-regulated SNARE proteins expression. Our study strongly suggested that CD36 depalmitoylation promoted its distribution from the plasma membrane to the lysosome and the CD36-UBQLN1-SNAREs complex formation, causing the downregulation of SNARE proteins in hepatocytes during sepsis. However, how CD36 recognized UBQLN1 and SNARE proteins has not yet been fully elucidated. Previous studies reported that CD36 ligand oleate triggers CD36 depalmitoylation and internalization facilitating oleate uptake in adipocytes [15]. It also remains unclear whether the engagement of a CD36 ligand was required for CD36 internalization and CD36-UBQLN1-SNAREs complex

formation in the process of sepsis. These questions will be addressed in future studies.

In conclusion, our findings provided fine evidence supporting that in response to sepsis, hepatocytes CD36 got depalmitoylated and translocated from the plasma membrane to the lysosome, where CD36 acted as a bridge molecule linking UBQLN1 to SNARE proteins and hence promoting the proteasomal degradation of SNARE proteins, which consequently contributed to septic liver injury. The present study not only reveals a novel function of CD36 linking ubiquitin-proteasome pathway to autophagy, but also suggests that inhibiting CD36 expression or targeting its palmitoylation in hepatocytes may represent a promising target to establish new pharmacological therapeutic strategies for septic liver injury.

Materials and methods

Human liver samples

Septic liver samples ($n=6$) were obtained from acute obstructive suppurative cholangitis (AOSC)-induced patients with sepsis at the Second Affiliated Hospital of Chongqing Medical University (Chongqing, China). Control liver samples ($n=6$) were obtained from patients with cholelithiasis. All AOSC-induced patients with sepsis and controls were between the ages of 18 and 80 years. The selection of AOSC-induced patients with sepsis was based on diagnostic criteria and severity assessment of acute cholangitis, using the Tokyo Guidelines and The Third 5 International Consensus Definitions for Sepsis and Septic Shock (Sepsis-3) [1]. Patients with a history of diabetes, alcohol use, viral hepatitis, or other chronic liver diseases were excluded from the study. The patients involved in this study underwent biliary drainage via percutaneous transhepatic catheter drainage. All procedures involving human sample collection and application were approved by the ethics committee of Chongqing Medical University and adhered to the principles of the Declaration of Helsinki. Informed consent for liver tissue analysis was obtained before the liver surgery.

Animals and treatment

All animals were maintained in a C57BL/6J background. *cd36*-HKO mice were generated for this study using the Cre-Loxp system. The *Cd36^{flox/flox}* mice were generated by using a plasmid with Loxp sites flanking *Cd36* exons 5. After electroporation, selection, and screening, properly targeted embryonic stem cell clones were injected into blastocyst for the generation of chimeric mice. Then, *Cd36^{flox/flox}* mice were crossed with *Alb* (albumin)-cre transgenic mice (Shanghai Model Organisms Center, China) to generate *cd36*-HKO mice.

C57BL/6J, *Cd36^{flox/flox}* and *cd36*-HKO mice aged 8 to 10 weeks were housed under controlled environmental conditions ($23 \pm 2^\circ\text{C}$) under a 12 h/12 h light/dark cycle, and allowed ad libitum access to water and a standard laboratory diet. To minimize variability and avoid any differences of food

intake, mice were deprived of food but free to water for 12 h before LPS (Sigma, L2630) or PBS (Biosharp, BL601A) treatment, as previously described [28], then mice ($n = 6$ for each group) were randomly assigned to receive intraperitoneal injection of PBS or LPS. The dosage of LPS injection was 12 mg/kg body weight. PBS-treated mice served as controls. After 12 h, the blood and tissues of mice were collected for further analysis.

Hepatocyte-specific *Ubqln1* OE mice were constructed by injecting with AAV8 by tail vein. The mouse *Ubqln1* coding sequence was cloned into an AAV vector under the control of a mouse *Alb* promoter (AAV8-*Apoe*). AAV8-*Apoe-Ubqln1* and AAV8-*Apoe*-null vectors were produced and titrated by GeneChem (Shanghai, China). Each mouse ($n = 6$ for each group) was injected with 1×10^{11} genome copies of AAV by tail vein. Four weeks later, these mice were treated with intraperitoneal injection of LPS (12 mg/kg).

All animal studies were performed in accordance with the guidelines of and approved by the animal care and use committee of Chongqing Medical University and followed NIH guidelines.

Cell culture and treatment

The human hepatocyte lines, HepG2 (American Type Culture Collection, HB-8065) and L02 (Kunming Institute of Zoology, Chinese Academy of Sciences, KCB 200511YJ), and HEK293T (American Type Culture Collection, ACS-4500) were cultured in DMEM (HyClone, SH30243.01) containing 10% fetal bovine serum (Natocor, SFBE) in an incubator at 37°C and 5% CO₂. Cells were treated with LPS at different concentrations according to the experimental design. Cells were stained with LysoSensor Green DND-189 dye (ThermoFisher Scientific, L7535) to determine the function of lysosome. The autophagic flux was measured using the mRFP-GFP-LC3 adenovirus (HanBio Technology, HB-AP210). Cells were transduced with mRFP-GFP-LC3 adenovirus for 48 h, and then treated with or without LPS for 24 h. The formation of autolysosome was detected and analyzed using a confocal microscope. The lysosome inhibitor CQ (Sigma, C6628) was used to pretreat cells for 2 h at the concentration of 50 μM. For inhibition of proteasomal degradation, cells were pretreated with LPS for 24 h, followed by proteasome inhibitor 3 μM MG132 (MedChemExpress, HY-13259) treatment for 12 h before harvest. To inhibit protein synthesis, cells were treated with 200 μg/mL cycloheximide (MedChemExpress, HY-12320) and LPS, and harvested at 0, 6, 12, 24 h. According to the manufacturer's instructions, cells were transfected with the siRNA (5 nM) against *UBQLN1* using Lipofectamine RNAiMAX Transfection Reagent (Invitrogen, 13778030). The siRNAs sequences were listed as follows: siTRIM38 (GUCCACAGCAAUGCGAAUATT), siTRIM25 (GCUCCUGGAGUAUUACAUTT), siUBQLN1 (CGGGAACUAAUGGAUCAATT). To inhibit the dephosphorylation of CD36, cells were treated with LPS and the dephosphorylation inhibitor LYPLA1 inhibitor ML348 (MedChemExpress, HY-100736, 5 μM) for 24 h.

Generation of knockout and overexpression cell lines

Stable *CD36* KO cells were established via a CRISPR-Cas9-sgRNA system. HepG2 and L02 cells were infected with lentiviral vectors carrying CRISPR-Cas9 and the two different *CD36*-targeted sgRNA (Genechem, China). These cells were selected with antibiotics to obtain two independent clonal *CD36* KO cell lines. The sgRNA1 sequences for *CD36* KO/*CD36* KO1 cells: GATGTTTCAGAACCTATTGA. The sgRNA2 sequences for *CD36* KO2 cells: ACCTTTATATGTGTCGATTA. The rescued KO cells were obtained by infecting *CD36* KO cells with the lentiviral (GV341) vector carrying WT-*CD36* cDNA.

As previously described (14), the lentiviral (GV341) vector carrying negative control (NC), WT-*CD36/CD36* OE cDNA and *CD36*[AA-SS] cDNA were synthesized from Genechem (Shanghai, China). HepG2 and L02 cells were infected with the multiplicity of infection of 10 and 15 respectively, and stable cell lines were selected with puromycin.

Plasmid construction

The pGV417 and pGV417-*UBQLN1* plasmids were purchased from GeneChem (GOSE0262889). Cells were transfected using Lipo8000™ (Beyotime Biotechnology, C0533) following the manufacturer's protocol.

Antibodies

We used the following antibodies: antibodies for *CD36* (Novus Biologicals, NB400-144; Novus Biologicals, NB600-1423), *CD36* Alexa Fluor® 488 (Santa Cruz Biotechnology, sc-7309; AF488), Albumin (Proteintech, 16475-1-AP), SQSTM1/p62 (Abcam, ab109012), LC3B (Abcam, ab192890), ACTB/β-ACTIN (ZSGB-BIO, TA-09), LAMP1 (Abcam, ab62562), RAB5 (Abcam, ab218624), IL1B (Genetex, GTX636887), IL6 (Genetex, GTX110527), TNF (Abcam, ab215188), cleaved-CASP3/caspase3 (Cell Signaling Technology, 9661), cleaved-CASP8/caspase8 (Cell Signaling Technology, 8592), STX17 (Genetex, GTX130212), SNAP29 (Santa Cruz Biotechnology, sc-390,602), VAMP8 (Abcam, ab76021), ubiquitin (Santa Cruz Biotechnology, sc-166,553; Proteintech, 10201-2-AP), FLAG (Cell Signaling Technology, 14793S), *UBQLN1*/ubiquitin 1 (Cell Signaling Technology, 14526S; abnova, H00029979-M02), HA (Cell Signaling Technology, 3724S), ATP1A1 (Proteintech, 55187-1-AP), and HRP-streptavidin (Sangon Biotech, D111054-0100).

Immunoblotting and immunoprecipitation-immunoblotting

Western blots were carried out on total protein extracts from cells and liver tissues using RIPA Lysis (Beyotime Biotechnology, P0013B) containing protease (Biomake, B14002) and phosphatase inhibitors (Biomake, B15002). Protein lysates were separated by SDS-PAGE and transferred to PVDF membranes. Protein bands were visualized using the ECL detection system (Advansta, K-12045-D50) with the

appropriate secondary antibodies: anti-rabbit HRP (ZSGB-BIO, ZB-2301), anti-mouse HRP (ZSGB-BIO, ZB-2305).

Cells were transfected or co-transfected with the indicated plasmids for 24 h and lysed with 500 μ L of NP-40 lysis buffer (Beyotime Biotechnology, P0013F). Then, the lysate was precleared with Protein A Magnetic Beads (Millipore, LSKMAGA10) for 120 min at 4°C and incubated overnight at 4°C with appropriate primary antibodies and IgG (Beyotime Biotechnology, A7028, A7016). Protein A magnetic beads were then added to capture the immunoprecipitates for 120 min at room temperature. Captured immunoprecipitates were subjected to SDS-PAGE for immunoblotting analysis with the indicated antibodies.

Quantitative PCR

Total RNA was isolated with RNAiso Plus (TaKaRa, 9108) and reverse transcribed into cDNA by using a PrimeScript® RT reagent kit (TaKaRa, DRR037A). The qPCR was carried out by using the CFX connect real-time system (Bio-Rad, USA) and the SYBR Green PCR Mix kit (TaKaRa, RR820A). The levels of *ACTB*/ β -actin or *Rplp0/36B4* mRNA were used for data normalization. Values of target genes were calculated by using the $2^{-\Delta\Delta Ct}$ method. The sequences of primers used were as follows:

Il1b (mouse): GCAACTGTTCTGAACTCAACT (F), ATCTTTTGGGGTCCGTC AACT (R); *Il6* (mouse): CCACG GCCTTCCCTACTTC (F), TTGGGAGTGGTA TCCTCTG TGA (R); *Tnf* (mouse): CCCTCACAC TCAGATCATCT TCT (F), GCTACGACGTGGGCTACAG (R); *Ccl2* (mouse): TTAAAAACCTGGATCGGAACCAA (F), GCATTAGCTT CAGATTTACGGGT (R); *Rplp0/36B4* (mouse): AGATTCG GGATATGCTGTTGGC (F), TCGGG TCCTAGACCAGT GTTC (R); *STX17* (human): GTGAAATTACGCCG TCTTGAAC (F), GATATT GGATC GGAGTTGCTGAA (R); *SNAP29* (human): AAAAGCTACA ATCCGTTTCGACG (F), TCTCGG ACTCGTACATGAGGG (R); *VAMP8* (human): TGTGCGGAACCTGCAAAGT (F), CTTCTGCG ATGTCGCTTTGAA (R); *ACTB* (human): CATGTACGT TGCTATCCAGGC (F), Reverse CTCCTTA ATGTCAC GCACGAT (R). Forward, F; Reverse, R.

Histological analysis and immunofluorescence staining

Paraffin-embedded liver sections were stained with H&E to evaluate the inflammation foci formation. For immunofluorescence staining, after incubation with the indicated primary antibodies overnight at 4°C, TRITC- or FITC-conjugated appropriate secondary antibodies (ZSGB-BIO, ZF-0316, ZF-0313, ZF-0311, ZF-0312) were added to the sections to visualize the staining. DAPI reagent (Beyotime Biotechnology, P0131) was used to counterstain the nuclei. The confocal images were obtained using confocal microscope (Leica, TCS SP8). The image analysis was performed with ImageJ software or NIS elements software.

Serum biochemistry analysis and LDH activity in the liver

Serum GOT1 and GPT were determined by an automatic biochemistry analyzer. LDH activity in liver homogenate was

determined by a colorimetric kinetic LDH Kit (Nanjing Jiancheng Bioengineering Company, A020-2-2), and the LDH activity was normalized by protein contents.

TUNEL assay

A standard TUNEL assay was applied to formalin fixed liver sections using a commercial TUNEL kit (Beyotime Biotechnology, C1098).

Electron microscopy

Fresh tissue and cells were placed in 4% glutaraldehyde overnight at 4°C. Ultrathin sections were cut and then stained. Images were acquired on a transmission electron microscope (JEM-1400PLUS, Japan Electron Optics Laboratory).

Detection of CD36 protein palmitoylation

Protein palmitoylation was assessed by IP and acyl-biotin exchange. Briefly, total protein was extracted using NP-40 lysis buffer (Beyotime Biotechnology, P0013F) with protease inhibitors (Biomake, B14002) and N-ethylmaleimide (Sigma, E1271). After precipitating CD36 protein with anti-CD36 antibody (Novus Biologicals, NB600-1423) and Protein A Magnetic Beads, samples were resuspended with stringent buffer (NP-40 lysis buffer containing 1.25 mg/ml N-ethylmaleimide and 0.1% SDS) and divided into two groups (HAM-, HAM+). All hydroxylamine (HAM)-samples received 0.5 ml/sample of lysis buffer (pH 7.2) and all HAM+ samples received 0.5 ml/sample of HAM buffer, and were rotated at room temperature for 50 min. Then samples were added with Biotin-BMCC buffer (Sangon Biotech, C100222), and rotated at 4°C for 50 min. Proteins were eluted from the beads by boiling in sample buffer and the cleared supernatants were resolved by SDS-PAGE and electro-transferred to PVDF membranes. For detecting palmitoylated CD36, membranes were incubated with HRP-conjugated anti-streptavidin (Sangon Biotech, D111054-0100) for 1 h at 37°C. For detecting total CD36, membranes were incubated with anti-CD36 (Novus Biologicals, NB400-144) and subsequent HRP-conjugated secondary antibody.

Statistical analysis

The analysis of all data was performed with 2-tailed Student's t-test or one-way ANOVA accompanied by post hoc t-tests (GraphPad Prism 8). $p \leq 0.05$ (2-tailed) was considered significant. Data are reported as mean \pm SEM.

Acknowledgments

The study was supported by grants from the National Natural Science Foundation of China (81970510, 82270608, 31971084, 82241040), Chongqing Natural Science Foundation (cstc2021ycjh-bgzxm0146), Talent Project of Chongqing (CQYC201905079), the Science Fund for The Youth Innovation Team of Chongqing Medical University (W0062) and the Talent Development Program of CQMU for Postgraduate (BJRC202116).

Disclosure statement

No potential conflict of interest was reported by the authors.

Funding

The work was supported by the National Natural Science Foundation of China [81970510, 82270608, 31971084, 82241040], Natural Science Foundation of Chongqing [cstc2021ycjh-bgzxm0146], Talent Project of Chongqing (CQYC201905079), the Science Fund for The Youth Innovation Team of Chongqing Medical University (W0062) and the Talent Development Program of CQMU for Postgraduate (BJRC202116).

ORCID

Lei Zhao  <http://orcid.org/0000-0002-8365-7774>

References

- [1] Singer M, Deutschman CS, Seymour CW, et al. The third international consensus definitions for sepsis and septic shock (Sepsis-3). *JAMA*. 2016 Feb 23;315(8):801–810. DOI:10.1001/jama.2016.0287
- [2] Yan J, Li S, Li S. The role of the liver in sepsis. *Int Rev Immunol*. 2014 Nov-Dec;33(6):498–510.
- [3] Zhao L, Li Y, Ding Q, et al. CD36 senses dietary lipids and regulates lipids homeostasis in the intestine. *Front Physiol*. 2021;12:669279.
- [4] Leelahavanichkul A, Bocharov AV, Kurlander R, et al. Class B scavenger receptor types I and II and CD36 targeting improves sepsis survival and acute outcomes in mice. *J Immunol*. 2012 Mar 15;188(6):2749–2758. DOI:10.4049/jimmunol.1003445
- [5] Choi AM, Ryter SW, Levine B. Autophagy in human health and disease. *N Engl J Med*. 2013 Feb 14;368(7):651–662.
- [6] Oami T, Watanabe E, Hatano M, et al. Blocking liver autophagy accelerates apoptosis and mitochondrial injury in hepatocytes and reduces time to mortality in a murine sepsis model. *Shock*. 2018 Oct;50(4):427–434.
- [7] Lalazar G, Ilyas G, Malik SA, et al. Autophagy confers resistance to lipopolysaccharide-induced mouse hepatocyte injury. *Am J Physiol Gastrointest Liver Physiol*. 2016 Sep 1;311(3):G377–386. DOI:10.1152/ajpgi.00124.2016
- [8] Watanabe E, Muenzer JT, Hawkins WG, et al. Sepsis induces extensive autophagic vacuolization in hepatocytes: a clinical and laboratory-based study. *Lab Invest*. 2009 May;89(5):549–561.
- [9] Lin CW, Lo S, Perng DS, et al. Complete activation of autophagic process attenuates liver injury and improves survival in septic mice. *Shock*. 2014 Mar;41(3):241–249.
- [10] Yu Q, Zou L, Yuan X, et al. Dexmedetomidine protects against septic liver injury by enhancing autophagy through activation of the AMPK/SIRT1 signaling pathway. *Front Pharmacol*. 2021;12:658677.
- [11] Cho HI, Kim SJ, Choi JW, et al. Genipin alleviates sepsis-induced liver injury by restoring autophagy. *Br J Pharmacol*. 2016 Mar;173(6):980–991.
- [12] Wang Y, Li L, Hou C, et al. SNARE-mediated membrane fusion in autophagy. *Semin Cell Dev Biol*. 2016 Dec;60:97–104.
- [13] Itakura E, Kishi-Itakura C, Mizushima N. The hairpin-type tail-anchored SNARE syntaxin 17 targets to autophagosomes for fusion with endosomes/lysosomes. *Cell*. 2012 Dec 7;151(6):1256–1269.
- [14] Zhao L, Zhang C, Luo X, et al. CD36 palmitoylation disrupts free fatty acid metabolism and promotes tissue inflammation in non-alcoholic steatohepatitis. *J Hepatol*. 2018 Sep;69(3):705–717.
- [15] Hao JW, Wang J, Guo H, et al. CD36 facilitates fatty acid uptake by dynamic palmitoylation-regulated endocytosis. *Nat Commun*. 2020 Sep 21;11(1):4765. DOI:10.1038/s41467-020-18565-8
- [16] Xia Y, Liu N, Xie X, et al. The macrophage-specific V-ATPase subunit ATP6V0D2 restricts inflammasome activation and bacterial infection by facilitating autophagosome-lysosome fusion. *Autophagy*. 2019 Jun;15(6):960–975.
- [17] Takats S, Nagy P, Varga A, et al. Autophagosomal Syntaxin17-dependent lysosomal degradation maintains neuronal function in *Drosophila*. *J Cell Biol*. 2013 May 13;201(4):531–539. DOI:10.1083/jcb.201211160
- [18] Mastrodonato V, Morelli E, Vaccari T. How to use a multipurpose SNARE: the emerging role of Snap29 in cellular health. *Cell Stress*. 2018 Mar 22;2(4):72–81.
- [19] Cornick S, Kumar M, Moreau F, et al. VAMP8-mediated MUC2 mucin exocytosis from colonic goblet cells maintains innate intestinal homeostasis. *Nat Commun*. 2019 Sep 20;10(1):4306. DOI:10.1038/s41467-019-11811-8
- [20] van Tol S, Atkins C, Bharaj P, et al. VAMP8 contributes to the TRIM6-mediated type I Interferon Antiviral Response during West Nile virus infection. *J Virol*. 2020 Jan 6;94(2):e01454. DOI:10.1128/JVI.01454-19
- [21] Wang YS, Tzeng HT, Tsai CH, et al. VAMP8, a vesicle-SNARE required for RAB37-mediated exocytosis, possesses a tumor metastasis suppressor function. *Cancer Lett*. 2018 Nov 28;437:79–88. DOI:10.1016/j.canlet.2018.08.023.
- [22] Pan JA, Sun Y, Jiang YP, et al. TRIM21 ubiquitylates SQSTM1/p62 and suppresses protein sequestration to regulate redox homeostasis. *Mol Cell*. 2016 Mar 3;61(5):720–733. DOI:10.1016/j.molcel.2016.02.007
- [23] Senturk M, Lin G, Zuo Z, et al. Ubiquitins regulate autophagic flux through mTOR signalling and lysosomal acidification. *Nat Cell Biol*. 2019 Mar;21(3):384–396.
- [24] N'diaye EN, Kajihara KK, Hsieh I, et al. PLIC proteins or ubiquitins regulate autophagy-dependent cell survival during nutrient starvation. *EMBO Rep*. 2009 Feb;10(2):173–179.
- [25] Rothenberg C, Srinivasan D, Mah L, et al. Ubiquitin functions in autophagy and is degraded by chaperone-mediated autophagy. *Hum Mol Genet*. 2010 Aug 15;19(16):3219–3232. DOI:10.1093/hmg/ddq231
- [26] Zeng S, Wu F, Chen M, et al. Inhibition of Fatty Acid Translocase (FAT/CD36) palmitoylation enhances hepatic fatty acid beta-oxidation by increasing its localization to mitochondria and interaction with long-chain Acyl-CoA synthetase 1. *Antioxid Redox Signal*. 2022 Jun;36(16–18):1081–1100.
- [27] Wang J, Hao JW, Wang X, et al. DHHC4 and DHHC5 facilitate fatty acid uptake by palmitoylating and targeting CD36 to the plasma membrane. *Cell Rep*. 2019 Jan 2;26(1):209–221 e5. DOI:10.1016/j.celrep.2018.12.022
- [28] Sun Y, Yao X, Zhang QJ, et al. Beclin-1-dependent autophagy protects the heart during sepsis. *Circulation*. 2018 Nov 13;138(20):2247–2262. DOI:10.1161/CIRCULATIONAHA.117.032821